Desalination xxx (xxxx) xxx–xxx

Contents lists available at ScienceDirect

Desalination

journal homepage: www.elsevier.com/locate/desal

Desalination properties of a free-standing, partially oxidized few-layer graphene membrane

Janardhan Balapanuru[a,b,1], Kiran Kumar Manga[a,b,1], Wei Fu[a], Ibrahim Abdelwahab[a], Guangrong Zhou[c], Mengxiong Li[c], Hongbin Lu[c], Kian Ping Loh[a,*]

[a] Department of Chemistry and Centre for Advanced 2D Materials (CA2DM), National University of Singapore, 3 Science Drive 3, 117543, Singapore
[b] Grafoid Inc., 945 Prince Street, Kingston, Ontario K7L0E9, Canada
[c] State Key Laboratory of Molecular Engineering of Polymers, Department of Macromolecular Science, Collaborative Innovation Centre of Polymers and Polymer Composites, Fudan University, 220 Handan Road, Shanghai 200433, China

GRAPHICAL ABSTRACT

Partially oxidized few-layer graphene oxide (POFG) sheets are laminated with acryl binder to form large-area, free-standing, membranes for high-performance forward osmosis. By controlling the interlayer distance of the sheets and their degree of oxidation, superior salt rejection and high water flux can be achieved.

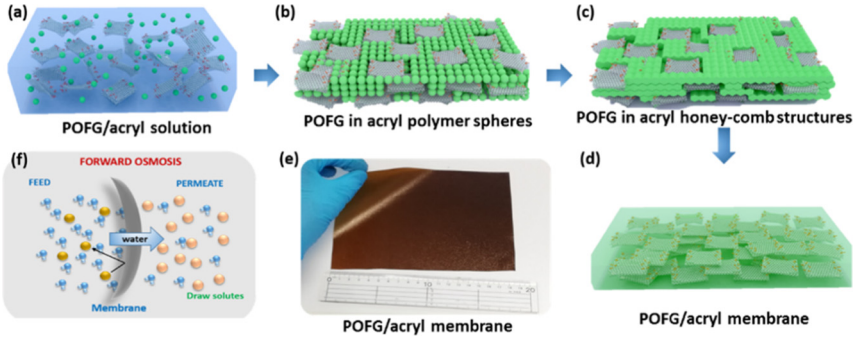

ARTICLE INFO

Keywords:
Graphene oxide
Few-layer graphene
Desalination
Free-standing membrane
Forward osmosis

ABSTRACT

Multi-stacked graphene oxide (GO) sheets containing intricate networks of microcapillary water channels are attractive as filtration membranes displaying both ultrahigh water permeation and ion exclusion properties. However, their practical utilization as desalination membranes is hampered by multiple issues, which include scalability, swelling of interlayer space, and mechanical instability under pressure-driven flux. To address these challenges, we have developed a process to laminate GO sheets with acryl binder to form large-area ($> 1\ m^2$ in lab) free-standing membranes for high-performance desalination. The key to high-performance desalination lies in the control of interlayer spacing in the graphene sheets and the controlled oxidation of graphene. Our results show that the performance of partially oxidized few-layer graphene (POFG) is much better than heavily oxidized GO in forward osmosis (FO) due to its smaller interlayer distance and resistance to swelling. Our acryl-laminated, POFG membrane (79 $L/m^2/h$ water flux, 3.4 $g/m^2/h$ reverse salt flux) performs at least seven times (with respective to the water flux) and three times (with respective to the reverse salt flux) better than that of commercial cellulose triacetate (CTA) membrane (10 $L/m^2/h$ and 12 $g/m^2/h$) in FO.

* Corresponding author.
E-mail address: chmlohkp@nus.edu.sg (K.P. Loh).
[1] Equal contributing authors.

https://doi.org/10.1016/j.desal.2018.08.005
Received 19 April 2018; Received in revised form 3 August 2018; Accepted 3 August 2018

1. Introduction

In the drive to alleviate water shortages caused by a growing population, seawater desalination and wastewater treatment are some of the most valuable technologies today [1]. In recent years, forward osmosis (FO) process has attracted growing interest in energy-efficient water desalination and wastewater treatment technologies. FO is driven mainly by osmotic pressure, thus it requires less energy input and has a lower fouling tendency compared to reverse osmosis (RO) [2]. The main drawback is the need to have a high concentration draw liquid. However, FO can find niche applications in the treatment of crude oil/water mixtures, the concentration of fruit juices, and biofuel wastewater treatments; these processes are not suitable for RO due to fouling tendencies when these concentrated liquids are purged through a RO cartridge [3]. Therefore, FO membranes combining the advantages of high water flux and high ion rejection are heavily demanded.

The ability of GO to form lamellar membranes with chemically tunable interfacial properties has stimulated interest in molecular sieving and desalination applications [4]. GO nanosheets can be assembled into laminar structures by vacuum filtration, drop-casting, spin-coating, and layer-by-layer (LBL) deposition methods, where a combination of electrostatic and van der Waals forces hold the sheets together [8,11,12]. However, most membranes prepared by these methods are mechanically fragile, thus they require additional support substrates, which limit the water flux of the FO membrane. For example, Rahman et al. [10] modified commercial thin-film composite (TFC) membrane support with Ag/GO composites. Some other examples include PAN-supported GO membranes [8] and PES-supported GO/Polypyrrole membranes [5]. Recently, Zhang et al. [11] reported a reduced graphene oxide (rGO)-based FO membrane that exhibits a higher water flux than commercial cellulose triacetate (CTA) membrane, but the preparation method involved tedious vacuum filtration and hydrogen iodide vapor reduction [11]. In most previous studies, when free-standing GO was used as the desalination membrane, the active testing area is restricted to only 2 mm^2. Although seldom explicitly stated, this is due to the poor stability of the membrane at larger length scale, where leakage paths due to cracks and pinholes would multiply [11]. Another problem is that when GO nanosheets are wetted, the infiltration of multilayer water increases the interlayer spacing of the nanosheets to > 9 Å. This permeation cut-off of ~9 Å is larger than the diameters of hydrated ions of common salts, which limits the use of GO nanosheets in desalination unless a method to physically confine the interlayers and prevent its expansion can be developed. Even though an epoxy-encapsulation method has been used to physically confine the GO and prevent swelling, the water flux performance (~0.5–5.6 L/m^2/h) becomes impractically low after the encapsulation [12].

To overcome the mechanical vulnerability as well as swelling of the stacked graphene sheets, researchers have attempted to embed GO sheets in various polymer matrixes [e.g., poly(vinylidene fluoride), polyethersulfone, etc.] to produce flexible and stable composite membranes [6,13,14]. Most of these polymer/GO membranes are prepared using phase-inversion methods that involve solvent/non-solvent exchange, in which the formation of grain boundaries (nanocorridors), voids and asymmetric structure (polymer rich on one side and GO on another side) is inevitable, leading to deleterious effects on the filtration performance. To alleviate these problems, an active layer (e.g., polyamide, PVA, etc.) can be coated on polymer/GO composite membranes (double-layer structure) [7,14,15]. Although such double-layer structure shows significant improvement in filtration, irreversible membrane-fouling induced by internal concentration polarization (ICP) limits their use in industrial applications [9].

Herein, we present a method of laminating partially oxidized few-layer graphene (POFG) using an acryl-based sealant to form a large-area, free-standing, POFG/acryl-membrane, which can address the problems of poor mechanical strength, scalability and swelling of GO membranes mentioned earlier. When tested in FO, the acryl-sealed POFG membrane shows higher water flux (79 L/m^2/h) and lower reverse salt flux (3.4 g/m^2/h) than commercial cellulose triacetate (CTA) membranes (water flux 10 L/m^2/h, reverse salt flux 12 g/m^2/h) [11] and its performances also exceeded those of other reported GO-based membranes [25–27].

2. Experimental methods and materials

2.1. Materials

Graphite flakes were purchased from Asbury Carbons Ltd. Sodium Nitrate ($NaNO_3$), Sulfuric acid (H_2SO_4), Hydrogen Peroxide (H_2O_2, 30%), Graphite rock, Lithium perchlorate ($LiClO_4$), Propylene carbonate, Carbon rod, Phosphoric acid (H_3PO_4) were purchased from Sigma Aldrich Pte. Ltd. The sealant-polymer solution was purchased from **Ronseal®** (**Type**: ***Satin***, a water-based acryl-polymer sealant).

2.2. Synthesis of graphene oxide (GO)

GO was synthesized from graphite through the modified-Hummers' method [24]. 1 g of graphite flakes (Asbury Carbons Ltd.) and 1 g of $NaNO_3$ were added to 500 mL round bottom flask and 45 mL of conc.

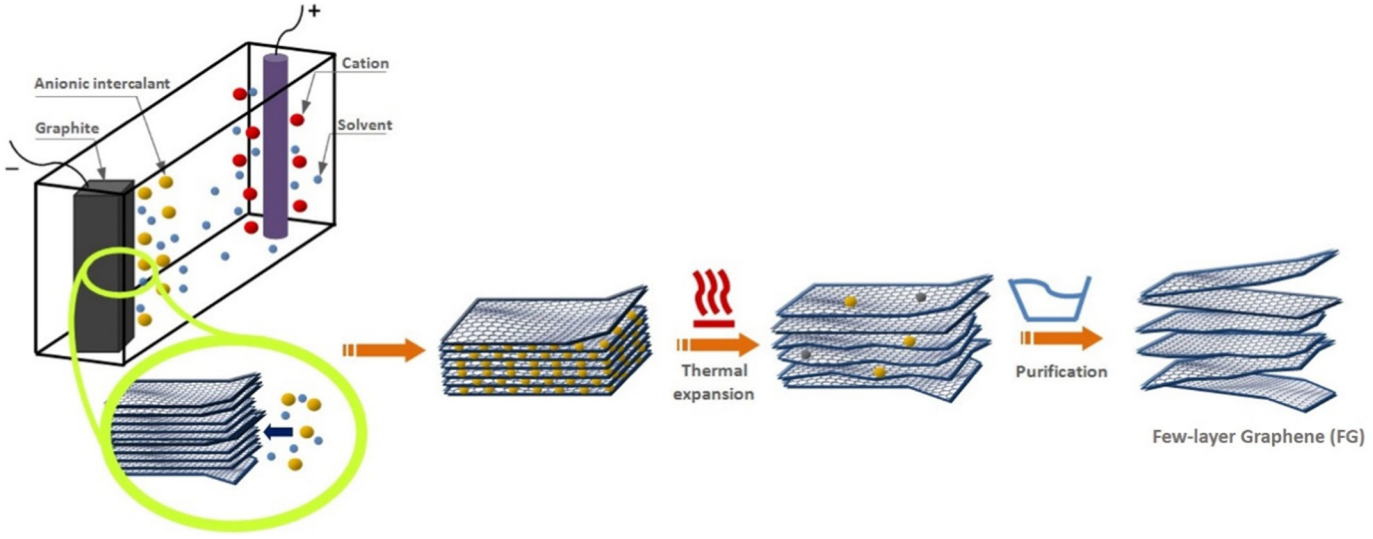

Scheme 1. Schematic illustration of Few-layer graphene synthesis.

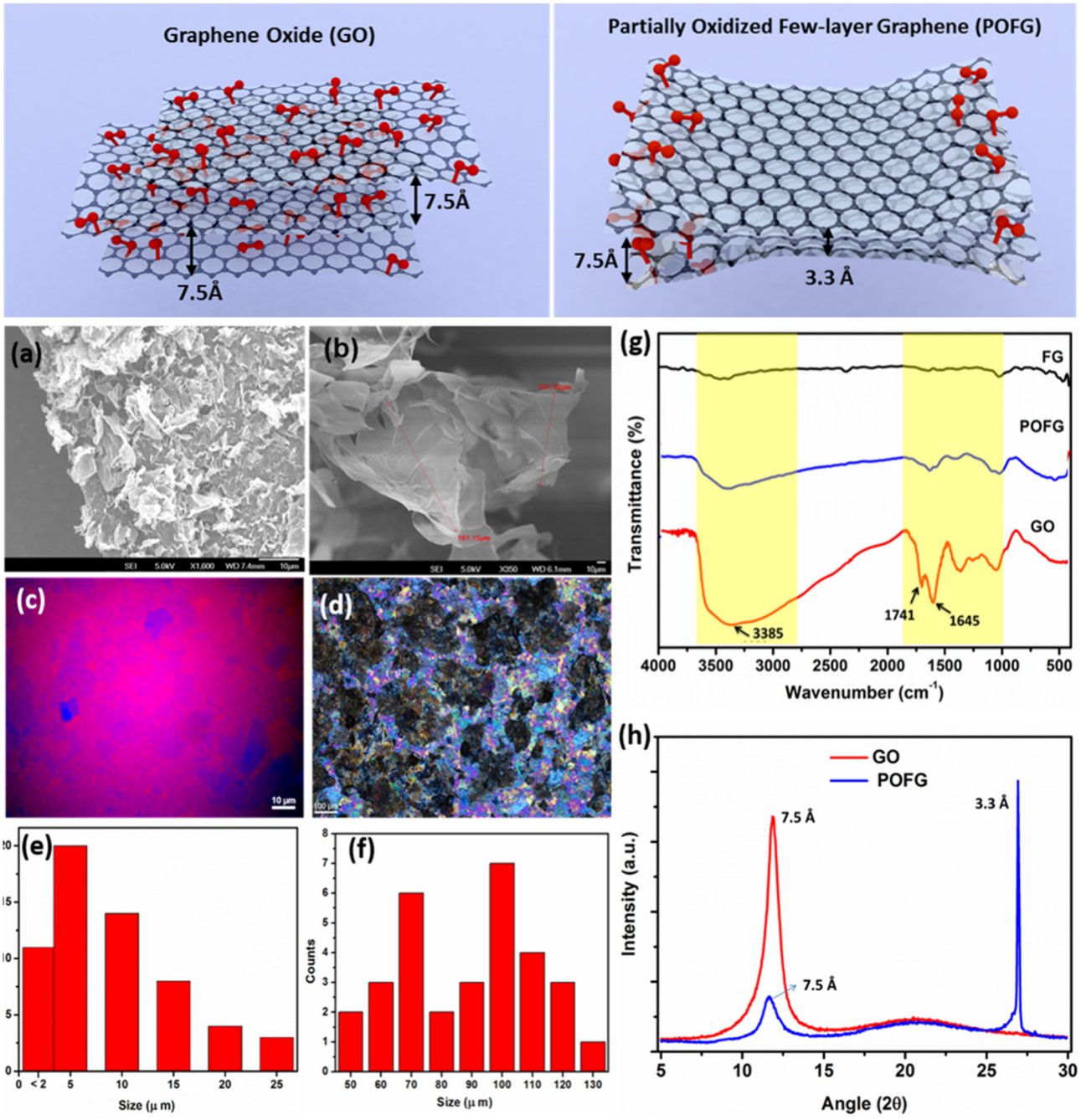

Fig. 1. Scanning electron microscopic (SEM) images of **(a)** exfoliated GO and **(b)** partially oxidized few-layer graphene (POFG); optical images and histograms of GO [**(c), (e)**] and POFG [**(d), (f)**], respectively; **(g)** FTIR Spectra of few-layer graphene (FG), POFG and GO showing variation in the oxidation and **(h)** powder-XRD analysis of GO and POFG.

H_2SO_4 was added to it. This mixture was allowed to stir for a few hours (3–4 h). Then 6 g of $KMnO_4$ was added slowly to the mixture at ice bath, to avoid rapid heat evolution. After 4 h, the flask was shifted to an oil bath and the reaction mixture was allowed to stir at 35 °C for 2 h, then temperature was increased to 60 °C and stirred for another 4 h. Finally, 40 mL of water was added to the reaction mixture (very slowly) and allowed to stir at 90 °C for 1 h, then the reaction was quenched by the addition of 10 mL of 30% H_2O_2. The warm solution was then filtered and washed with de-ionised water (DI water). The solid was dissolved in DI water and sonicated for 2 h to exfoliate the oxidized graphene sheets. The solution was centrifuged at 1000 rpm for 2 min to remove all the visible graphite particles, and then centrifuged at 13000 rpm for 2 h. These steps were continued until the pH of supernatant was 4–5.

2.3. Synthesis of few-layer graphene (FG)

Graphite rock (~0.5 Kg, < 10 Ω) was used as the negative electrode and electrochemically charged at a voltage of 15 ± 5 V in a 30 mg/mL solution of $LiClO_4$ in propylene carbonate (PC). Carbon rod (or lithium flake) was used as the positive electrode. During the electrochemical charging, HCl/DMF (50 mL/50 mL) (HCl used: 1 M) solution was used to remove the solid by products. Following the electrochemical charging, the expanded graphite was transferred into a glass Suslick cell (15 mL), followed by the addition of 50 mg/mL of LiCl in DMF solution (10 mL), PC (2 mL) and TMA (1 mL). The mixture was then sonicated for > 10 h (70% amplitude modulation, Sonics VCX750, 20 kHz) with an ultrasonic intensity of ~100 W/cm^2 (note that laboratory bath

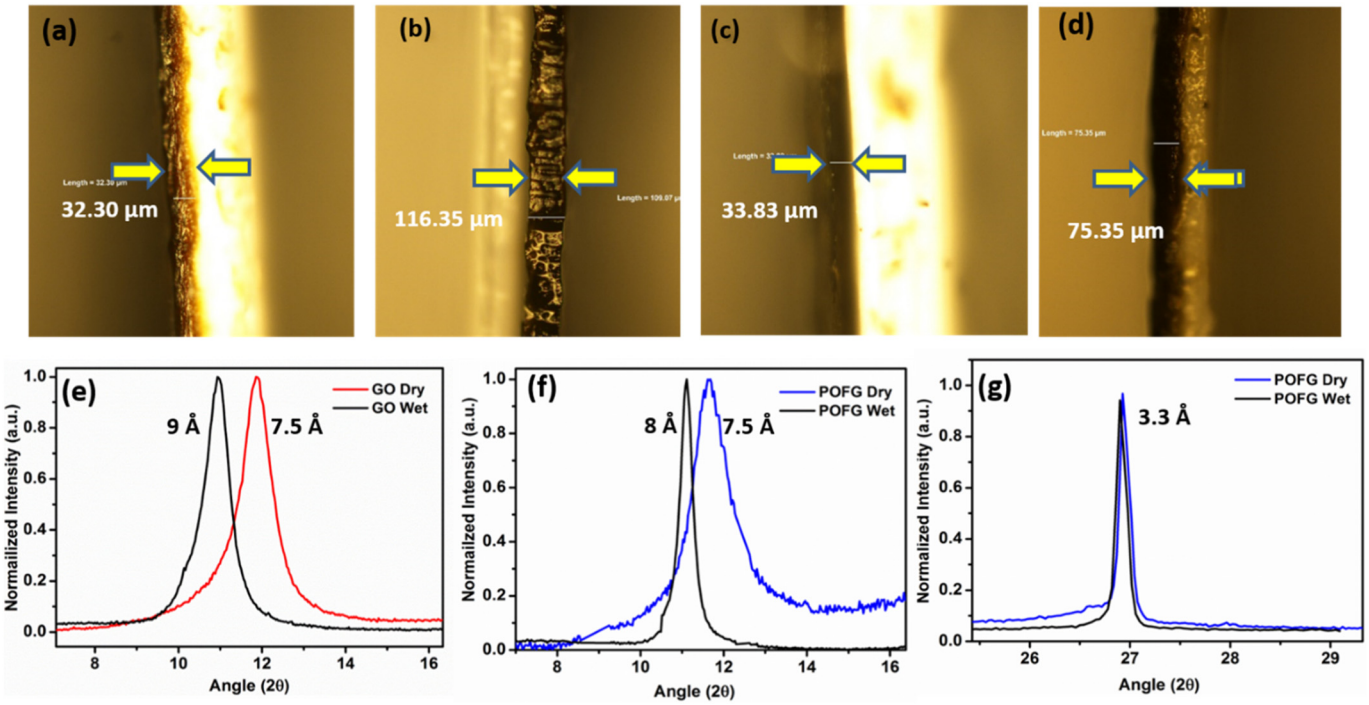

Fig. 2. Optical microscopic images of GO and POFG films: **(a)** Dry GO film, **(b)** GO film after soaking 4 days in DI water **(c)** Dry POFG film **(d)** POFG film after soaking 4 days in DI water; **(e)** XRD analysis of GO films after immersion in water; **(f), (g)** after immersion of POFG films in water and tracking XRD peak shifts for the 7.5 Å and 3.3 Å peaks in POFG.

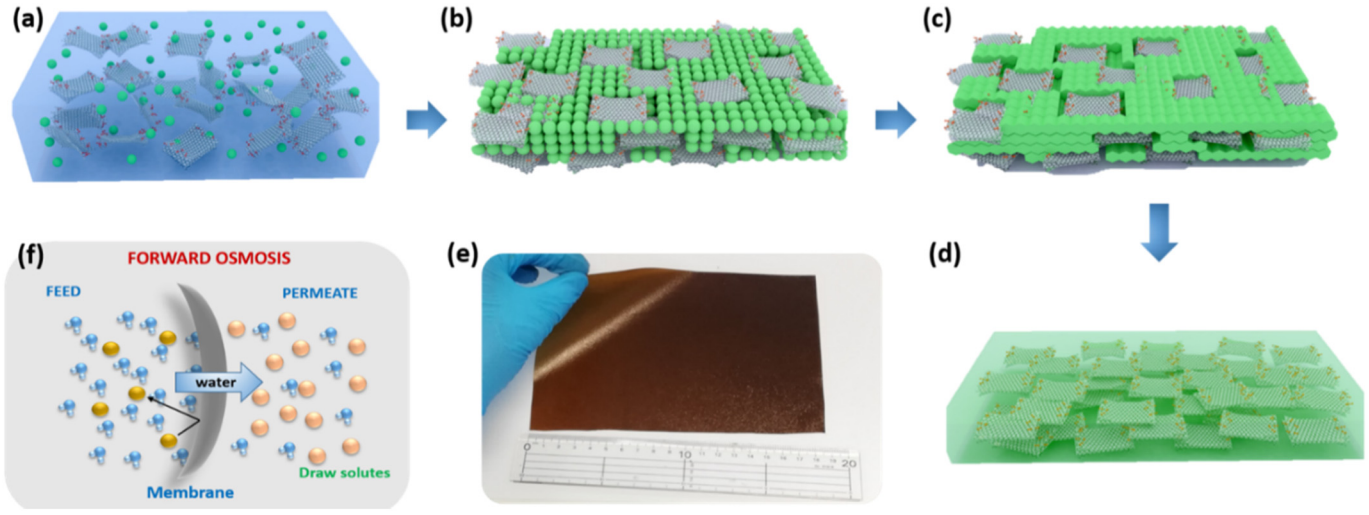

Scheme 2. Schematic illustration of the POFG/acryl membrane drying process. **(a)** POFG/acryl solution **(b)** POFG sheets embedded in acryl-polymer spheres **(c)** POFG sheets embedded in acryl-polymer honeycomb patterns **(d)** Continuous POFG/acryl membrane formation **(e)** large-area POFG/acryl membrane (20 cm × 15 cm) **(f)** Schematic illustration of FO process.

sonication may not work well due to low ultrasonic intensity).

The sonicated graphene powder was washed by HCl/DMF and several polar solvents of DMF, ammonia, water, isopropanol and THF, respectively. The grey-black graphene powder was collected by centrifugation or/and filtering during the washing. The graphite flakes were thermally expanded to form few-layer graphene (FG) by subjecting it to microwave treatment (for 2 min) in a domestic microwave oven (Panasonic, 1100 W) [19].

2.4. Synthesis of partially oxidized few-layer graphene (POFG)

1 g of few-layer graphene (FG) was suspended in 100 mL of concentrated H_2SO_4/H_3PO_4 (90:10 mL) and stirred for 30 min and 5.6 g $KMnO_4$ was added slowly to the mixture followed by stirring at room temperature for 1 h. Later, the reaction was quenched using 30% H_2O_2 (5 mL) and washed via centrifugation at 10000 rpm till the pH of the supernatant reached to 4–5. Using the same reaction conditions, the process could be scaled-up to > 1 Kg, but care must be taken while adding $KMnO_4$ to the acid mixture. The as-obtained POFG flakes have a typical thickness of 2.5–4.7 nm (corresponds to 3–5 layers; **Fig. S1**.) with a yield of 40%.

2.5. Synthesis of GO/Acryl and POFG/Acryl Composites

GO/Acryl composite solutions were prepared by blending GO with different amounts of water-based polymer solution (5 to 20 vol%). For

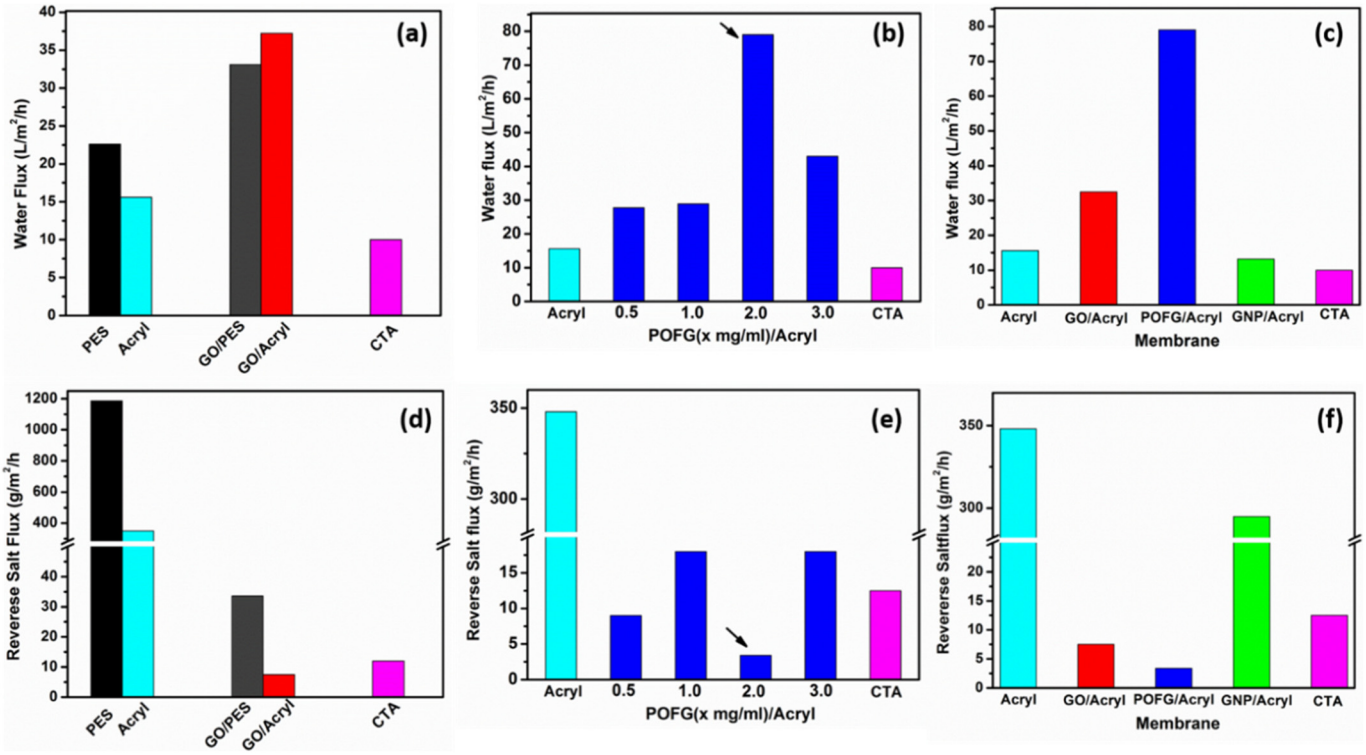

Fig. 3. Comparative FO performance: **(a–c)** Water flux and **(d–f)** reverse salt flux of the various membranes.

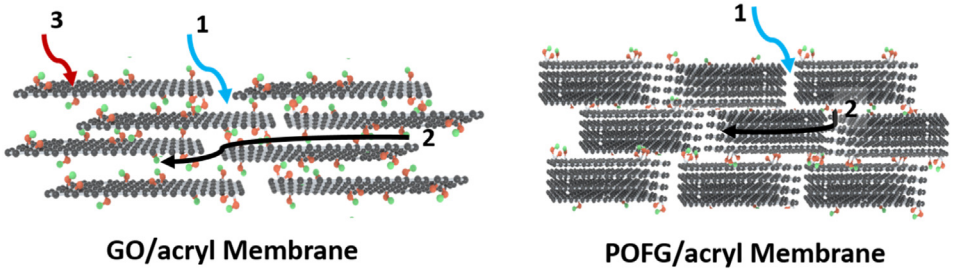

Scheme 3. Schematic illustration of diffusion pathways in GO/acryl and POFG/acryl membranes. Diffusion Pathways: 1. edges of the sheets; 2. inter-layer spacing and 3. defects or pores.

example, 7 vol% GO/Acryl composite prepared by mixing 0.7 mL of acryl polymer solution into 9.3 mL of GO (2 mg/mL) solution and stirred at room temperature for 24 h. Similar procedures were adopted to prepare POFG/Acryl composites. 7 vol% POFG/Acryl composite was prepared by mixing 0.7 mL of acryl polymer solution into 9.3 mL of POFG (2 mg/mL) solution and stirred at room temperature for 24 h.

2.6. Fabrication of GO/acryl and POFG/acryl free-standing membrane

The as-prepared GO/Acryl composite solution was casted on a polypropylene-coated surface and allowed to dry at room temperature for 24 h. Finally, free-standing GO/Acryl membrane was peeled-off the from the substrate polymer surface. POFG/Acryl membrane was also fabricated the same way. (Schematic illustration of the fabrication technique was presented in Supporting Information **Scheme S2**).

3. Results and discussion

3.1. Characterization of the GO, POFG

There are three possible pathways for the movement of sub-nanometer particles (e.g., hydrated ions) through stacked sheets of GO, namely: the ions can diffuse through pores, inter-edge areas and/or interlayer nanochannels [16]. It is difficult to control the size of the pores and the inter-edge areas, so using large GO sheets with lateral size > 100 μm, along with a binding material to provide the necessary cohesive forces, can reduce unwanted leakage paths [21]. To improve the filtration properties further, the wetting properties of the capillary channels can be tuned by chemical treatment. The hydrophilic and hydrophobic tracks in the channels act synergistically to enhance a high water flux. The permeation of water is mediated by the oxygenated domains (high surface tension), and its near-zero friction flow occurs through the pristine graphene regions (low surface tension) [17].

To study the correlation between hydrophobicity in the channels and FO performance, two types of GO were synthesized, namely, fully oxidized GO and partially oxidized few-layer graphene (POFG). The fully oxidized GO was synthesized by the conventional Hummer's method [24], whereas POFG was synthesized by the mild oxidation of electrochemically exfoliated few-layer graphene flakes from graphite [19] (Methods and Materials section Scheme 1). Scanning Electron Microscopy (SEM) and optical images in Fig. 1(a–f) show that POFG sheets have larger flake-size distribution (70–110 μm) compared to GO (2–15 μm). This is because of its preparation method which avoids vigorous oxidation conditions that cause fragmentation in GO sheets.[21]

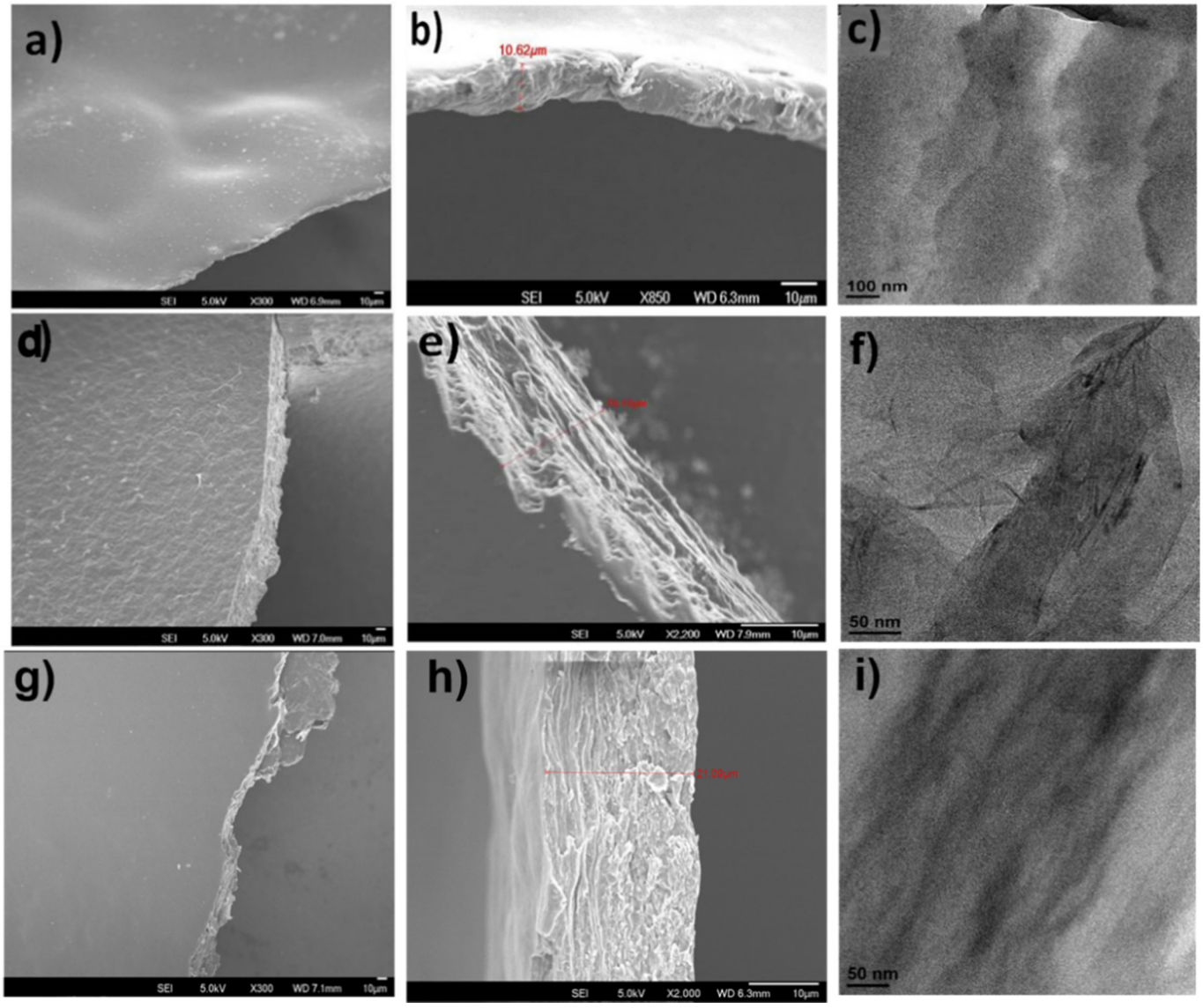

Fig. 4. SEM images of **(a, b)** pure acryl, **(d, e)** GO/acryl (7 vol%) composite and **(g, h)** POFG/acryl (7 vol%) membranes. Cross-section TEM imaging of **(c)** pure acryl **(f)** GO/acryl and **(i)** POFG/acryl membranes.

POFG flakes have a typical thickness of 2.5 to 4.7 nm as determined by AFM, which corresponds to between 3 and 5 layers of graphene (Supporting Information **Fig. S1**). The differing degrees of oxidation in GO and POFG have been investigated by Fourier Transform Infrared (FTIR) analysis. Fig. 1(g) shows that the intensities of peaks corresponding to C═O (1741 cm^{-1}) and –OH (3385 cm^{-1}) vibrations are lower in POFG than in fully oxidized GO (Normalized FTIR data is presented in Supporting Information (**Fig. S2**)). This is also supported by the thermogravimetric analysis (TGA) data of GO and POFG (See **Fig. S3** in supporting information) where POFG shows higher thermal stability than that of GO. The milder oxidation process used in the preparation of POFG enabled us to achieve edge functionalization while maintaining a pristine graphene basal plane. The Raman spectra of POFG and GO (Supporting Information **Fig.S4**) also confirms that POFG contains less oxidative defects compared to that of GO. The intensity ratio of D band over G band (I_D/I_G) reflects the extent of structural defects and disorder in graphene materials [30]. As shown in **Fig. S4**. the I_D/I_G value for GO is ~0.91 whereas for POFG it is ~0.48, which indicates that POFG is less defective compared to that of GO [30]. The relatively stronger 2D peak at 2704 cm^{-1} for POFG also represents its more ordered structure compared to that of GO.

The presence of oxygen functional groups on the basal plane of GO imposes steric repulsion effects, which causes the interlayer distance in stacked GO sheets to widen. Thus, both hydrophilic effects and a larger interlayer distance will cause a greater infiltration of water in GO compared to the POFG samples. The interlayer distances of POFG and GO have been investigated using powder XRD. As shown in Fig. 1(h), the interlayer spacing in restacked GO sheets is 7.5 Å, which is consistent with previous reports.[18] The XRD spectrum of POFG in Fig. 1(h) shows two peaks: the interlayer spacing of 7.5 Å corresponds to the oxidized edges, similar to that present in the oxidized GO, while the 3.3 Å spacing is characteristic of tightly packed graphene layers in the inner regions [19,23]. It is understood that the minimum cut-off interlayer spacing to block monovalent hydrated ions is 6.4 Å and 7.2 Å for K^+ and Na^+ respectively [12]; thus, it can be expected that POFG should offer size-exclusion effects to the hydrated ions due to its smaller interlayer spacing.

In addition, it is important to study the swelling behavior of pure GO and POFG films (in water) to assess their long-term stability [18]. To do so, we have soaked the GO and POFG free-standing films for 4 days in deionized water, and the swelling behavior was visually captured by the optical spectroscope. As shown in Fig. 2(c, d), the

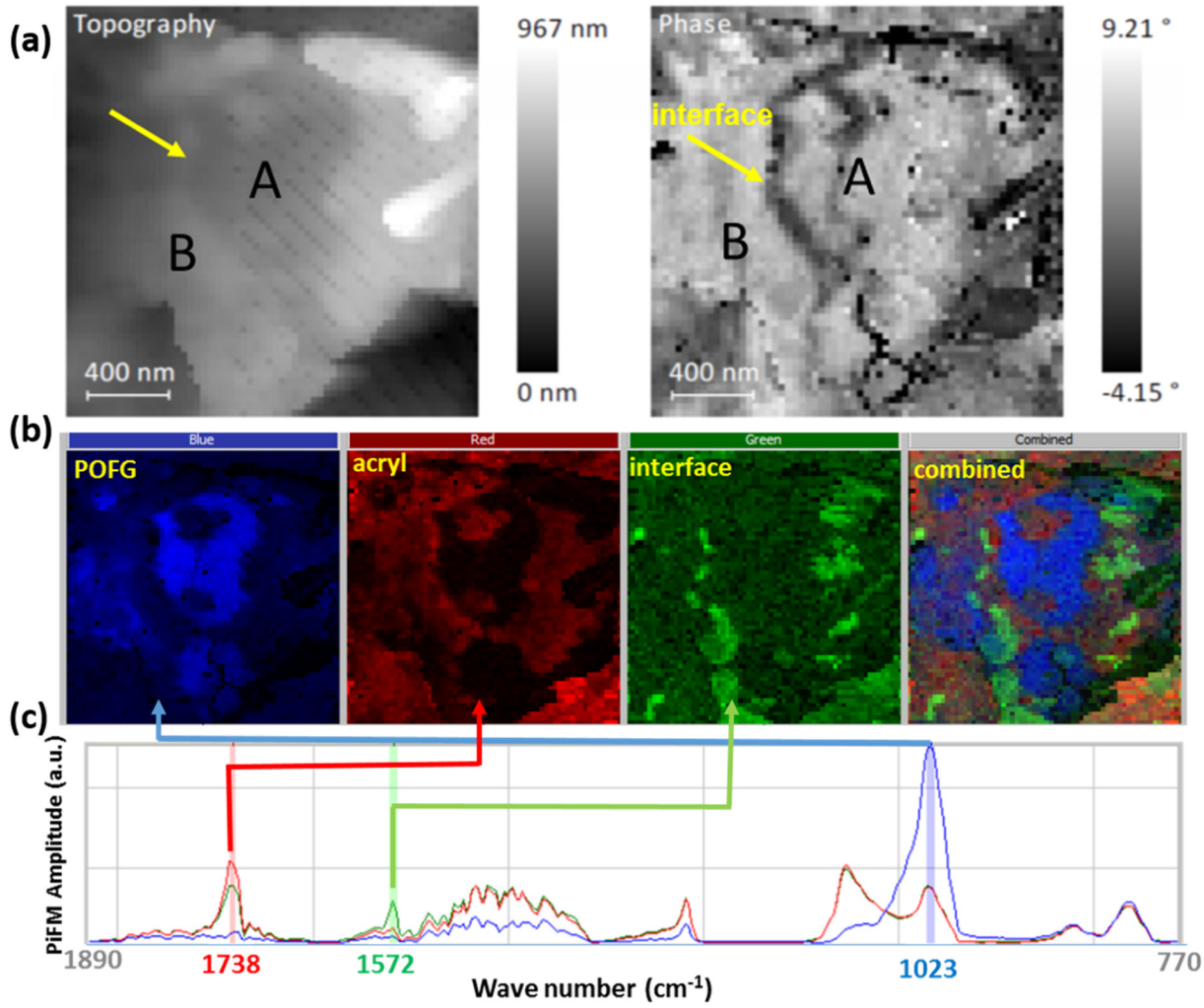

Fig. 5. Photo-induced Force Microscopy (PiFM) imaging of POFG/acryl membrane: **(a)** Topographic and phase images of the selected region. **(c)** A hyperspectral IR (hyPIR) acquired from 770–1890 cm^{-1} with an image of the PiFM response at all wavenumbers and **(b)** PiFM imaging acquired by tuning the laser to specific wavenumbers at 1023, 1738 and 1572 cm^{-1}.

increase in thickness of POFG is about two times smaller (thickness change from 33.8 µm to 75.3 µm) compared to that of GO Fig. 2(a, b) (thickness change from 33.3 µm to 116.3 µm), which confirms the smaller inter-plane distance as well as larger hydrophobicity of POFG [17]. To confirm the changes in inter-layer spacing, we have carried out XRD analysis of these samples after immersion in water, where the interlayer spacing in GO was found to increase from 7.5 Å to 9 Å (Fig. 2(e)). POFG film is characterized by two interlayer spacings. There is only a 0.5 Å increment in POFG film (Fig. 2(f)) for the 7.5 Å peak and an insignificant change for the 3.3 Å peak (Fig. 2(g)), thus confirming that the smaller interlayer spacing in POFG resists swelling.

To improve the stability of GO-based membranes, polymer matrixes (PES, PVDF, PSf, etc.) prepared using the phase-inversion preparation method had been used by various researchers to form composites with GO [14,15]. Even though the water flux of the composite membranes was improved, the salt-rejection property became poorer relative to the pure GO membrane due to the presence of microvoids and grain boundaries. In addition, the phase segregation of GO occurred due to hydrophilic (GO)/hydrophobic (polymer) incompatibility, which created voids on one side and a dense layer on the other side, leading to internal concentration polarization (ICP) in ionic solutions. Clearly, there is a need to identify a polymer that allows homogeneous distribution of GO and forms void-free interfaces. Our search brings us to an acrylic-based water-soluble polymer that can be cured by a room-temperature drying process.

3.2. Fabrication Process of GO or POFG/acryl Membrane

The same membrane fabrication process applies to both GO or POFG, thus selecting either GO or POFG allows us to study the role of hydrophobicity/hydrophilicity in desalination. First, POFG/acryl composite solution was cast on a polypropylene-coated surface and allowed to dry for 24 h at room temperature. The typical drying process (Scheme 2) of this polymer involves evaporation of solvent (water), which leads to the formation of microscopic acrylic polymer spheres. Subsequently, these spheres self-assemble into a honeycomb-like pattern by capillary forces, and the attractive forces between the spheres leads to the deformation and coalescence of the spheres. As shown in the above schematic, acrylic polymer spheres bind onto the POFG surface via hydrogen bonding interactions and polar-polar interactions [20] between the ester groups of polyacrylate and oxygen functionalities of POFG sheets [20]. Upon solvent evaporation, the polymer spheres coalesced and laminated the embedded POFG into a continuous POFG/acryl cohesive film. The air-dried membrane film was subsequently peeled off from the polypropylene surface and was used without any further modifications. The advantage of this method is its scalability. On the bench top, we can easily fabricate a 20 cm × 15 cm membrane using an aqueous-based process (Scheme 2(e)). POFG/acryl membranes of different compositions were fabricated by varying the composition of acryl to POFG (5 vol% to 20 vol% of acryl in POFG) and

tested for FO performance (Supporting Information **Table S1**).

3.3. GO/polyethersulfone (PES) membrane fabrication

For comparison, we fabricated GO-PES membranes via the standard phase-inversion method. In a typical process, a GO-PES composite solution (e.g., GO (1 wt%) + PES (20 wt%) + Polyvinylpyrrolidone (1 wt %) + DMF solvent) was cast on a supporting layer (glass) and then submerged in a coagulation bath containing a non-solvent (DI water). Due to the solvent and non-solvent exchange, precipitation occurs as shown in **Fig. S6.** The prepared membranes from the above two processes (Acryl sealing and phase-inversion) were tested in FO using 2 M NaCl solution as a draw and DI water as a feed solution.

3.4. Forward osmosis performance

Fig. 3 shows the water flux and reverse salt flux performance of various membranes. The active testing area for FO is standardized at 2 cm^2 for all. In general, a high water flux has to be matched by a low reverse salt flux for good desalination performance. The desalination membrane prepared via the acryl sealing process (GO/acryl) shows a lower salt permeation (7.5 $g/m^2/h$) (Fig. 3(d)) compared to membranes prepared using the phase-inversion method (GO/PES, 33.6 $g/m^2/h$) and commercial cellulose triacetate (CTA) membrane (12 $g/m^2/h$) [11]. The superior performance of POFG/acryl membrane is attributed to the efficient sealing ability of acryl binder at the POFG-acryl interface. The pure acrylic polymer membrane has a much lower water flux than GO-acryl (Fig. 3(a)) and POFG-acryl composite membrane (Fig. 3(c)), which means water permeates mostly through the GO or POFG interlayer channels. The efficient sealing between POFG and acryl should be due to their functional group interactions and compatibility. The salt rejection ability is ascribed to the interlayer distance in confined POFG, which affords the appropriate size exclusion effect for hydrated Na^+. In contrast, in the case of GO/PES membrane, salt ions permeate through both voids created at GO-PES interface and the PES matrix, leading to a higher salt leakage compared to the GO/acryl membrane.

The hydrophilicity of GO allows highly efficient permeation of water molecules; hence, it is unsurprising to see improvement in water flux for both GO/PES and GO/acryl membranes compared to the polymer-alone membranes (PES, acryl membranes respectively). As shown in Fig. 3(a), GO/acryl membrane (37.2 $L/m^2/h$) shows better water permeability compared to the GO/PES membrane (33.1 $L/m^2/h$). The improved water flux in the GO/acryl membrane is attributed to its symmetric membrane structure with uniform dispersion of GO sheets, which creates a network of channels for water transport. In contrast, in GO/PES, the membrane phase segregates into polymer-rich hydrophobic regions and hydrophilic regions, which creates a larger diffusion barrier for water transport. The asymmetric structure in the GO/PES membrane further leads to internal concentration polarization (ICP), which also affects the water permeability. Hence, acryl-laminated GO membranes show better performance in desalination compared to GO membranes made by conventional phase-inversion methods. The acryl-lamination method was further extended to different types of graphene derivatives: POFG and graphene nanoplatelets (GNP).

The effect of hydrophobicity of the GO on the FO performance was investigated next. Fig. 3(c) shows that the POFG/acryl membrane shows the highest water flux ((79 $L/m^2/h$), Fig. 3(b, e)) and lowest reverse salt flux (3.4 $g/m^2/h$) among all composite membranes tested (Fig. 3(f)), including GO/acryl (32.5 $L/m^2/h$ and 7.5 $g/m^2/h$), GNP/acryl (13.2 $L/m^2/h$ and 294.8 $g/m^2/h$) and commercial membrane cellulose triacetate (CTA) (water flux 10 $L/m^2/h$, reverse salt flux 12 $g/m^2/h$) [11]. The water flux performance of the POFG/acryl membrane is significantly higher than that of other reported graphene-based membranes (for rGO membrane: [11] 57 $L/m^2/h$, GO-polyamide/polysulfone membrane: [25] 34.7 $L/m^2/h$, polyvinylpyrrolidone modified GO membrane: [26] 33.2 $L/m^2/h$, CN/rGO membrane: [27] 41.4 $L/m^2/h$). The good performance of POFG originates from several unique features: its flake size is much larger, and it also has larger regions of hydrophobic channels compared to fully oxidized GO (Fig. 1).

Theoretical studies have shown that friction-free water transport across the membrane takes place via non-oxidized nanochannels in GO [16,28,29]. The salt-retention performance of the POFG/acryl membrane is attributed to its large flake size and close-packed structure, which presents more trapping sites for ions compared to fully oxidized GO, the latter has a relatively loose packing structure. The POFG/acryl membrane has good tortuosity due to the convoluted path for ions through the channels and edges, as illustrated in (Scheme 3). It should be noted that if unoxidized graphite nanoplatelets (GNP) were used to make a GNP/acryl composite FO membrane using the same method for POFG/acryl, a much poorer performance was obtained. This suggests that some degree of oxygenation of the graphene is required to help with dispersion of the flake and to allow a high water flux.

Fig. 4 shows the surface and cross-sectional morphologies of pure acryl, GO/acryl and POFG/acryl membranes. Compared to the POFG/acryl membrane, the surface of the GO/acryl membrane (Fig. 4(c)) appears to be rough, which is due to the more convoluted, disordered structure of the restacked GO sheets present in the acryl matrix. In contrast, a very smooth surface was observed for the POFG/acryl membrane (Fig. 4(e)). The larger sized POFG and its stronger π-π stacking (and hence smaller interlayer distance) may be responsible for the highly ordered, layered stacking structure of POFG.

Probing the inner structures of the membrane may offer clues to the variation of performance among the different composite membranes. Using cross-section SEM, we observed that the pure acryl (Fig. 4(a–b)) membrane does not have a layered structure. In contrast, the cross-sectional morphologies of GO/acryl and POFG/acryl composite membranes (Fig. 4(e), (h)) reveal lamellar structures. We have prepared ultrathin samples for TEM imaging using a microtome equipped with a diamond knife. As shown in Fig. 4(f), the POFG/acryl membrane has a homogeneous distribution of POFG, whereas the GO/acryl membrane has a random distribution of GO.

3.5. Nano-FTIR Imaging of POFG/acryl Membrane

To probe the nature of chemical bonding between the polymer and POFG at the phase boundary, a nano-FTIR imaging technique was used to perform chemical imaging. Here, we applied Photoinduced Force Microscopy (PiFM) to generate local IR absorption spectra with lateral resolution better than 10 nm and within a probing depth that is limited to 10 nm.

The chemical and morphological structure of the interface between POFG and acryl-binder was probed by hyperspectral IR (hyPIR) imaging [22], where PiFM spectra are acquired for each pixel of an (n × n) array with the laser tuned to the different wavenumbers that correspond to the various absorption peaks of the POFG and acryl-binder.

Fig. 5(a) shows the topography and phase images of a selected portion of the POFG/acryl membrane where the POFG and acryl-binder regions could be differentiated, and labeled **A** and **B**, respectively, with a clear interface as it appeared in the phase image. We have performed hyPIR mapping (Fig. 5(c)) from 770 cm^{-1} to 1890 cm^{-1}, which is the fingerprint region for various functional groups. For example, we have selected 1023 cm^{-1} (blue) and 1738 cm^{-1} (red) for the scanning wavenumbers to differentiate POFG and acryl, since these are the fingerprints regions for the −C−O− stretch in POFG and the $COOCH_3$ stretch in acryl (stretch), respectively (Fig. 1, **Fig. S4**). The spatial maps scanned at these specific wavenumbers are shown in Fig. 5(b), where the blue map at 1023 cm^{-1} is a marker for the dispersed POFG sheets in acryl polymer, whereas the red map at 1738 cm^{-1} represents the acryl polymer. Interestingly, when we scanned at 1572 cm^{-1}, the corresponding green image was found at the interface between the POFG and acryl polymer; this is assignable to the −C=O stretching of the edge carboxylate groups of POFG, which strongly interacts with −(COOR) of

acryl ester groups through hydrogen bonding and other polar-polar interactions [20a]. Thus, interfacial bonding between the two phases provides the sealing needed to prevent ions from leaking through the phase boundary regions.

4. Conclusions

We have developed a method of laminating partially oxidized few-layer graphene (POFG) sheets with an acryl-based sealant to fabricate large-area, free-standing high-performance GO-based membranes for filtration applications. We observed that desalination membranes constructed from few-layered graphene flakes synthesized by a low-oxidation route exhibit better desalination performance than that made using conventional GO materials. The good performance of POFG membranes was due to its smaller interlayer distance, higher hydrophobicity and swelling resistance. Our study addressed three critical issues facing GO-based membranes in desalination applications: (i) scalability, (ii) mechanical stability of the GO-based free-standing membranes, and (iii) a high water flux/salt rejection ratio. By using an acryl-laminated POFG membrane, we are able to achieve high water flux while maintaining salt retention performance at least 7 times higher than the conventional CTA membranes and ~2–3 times better than that of GO membranes. Most importantly, our fabrication process is readily scalable to large-sized membranes, thus making it useful for industrial level nanofiltration and wastewater treatment applications.

Acknowledgements

K. P. Loh acknowledges support from National Research Foundation, Prime Minister's Office, NRF mid-investigator award NRF-NRFI2015-01 “Graphene Oxide – A new class of catalytic, ionic and molecular sieving material”. We are thankful to Prof. Xie Jianping and Mr. Li Jingguo from Department of Chemical and Biomolecular Engineering, NUS to help us do initial trail runs. The authors would like to thank Will Morrison, Dr. Thomas Albrecht and Dr. Sung Park from Molecular Vista Inc. for their help with the PiFM measurements. We also acknowledge the help from Mr. Ho Quang Binh to draw the schematic for the electrochemical exfoliation of graphite (Scheme 1).

Appendix A. Supplementary data

Supplementary data to this article can be found online at https://doi.org/10.1016/j.desal.2018.08.005.

References

[1] (a) A.S. Mark, W.B. Paul, E. Menachem, G.G. John, J.M. Benito, M.M. Anne, Science and technology for water purification in the coming decades, Nature 452 (2008) 301–310;
(b) Y. Wang, L. Li, Y. Wei, J. Xue, H. Chen, L. Ding, J. Caro, H. Wang, Water transport with ultralow friction through partially exfoliated g-C_3N_4 nanosheet membranes with self-supporting spacers, Angew. Chem. Int. Ed. 56 (2017) 8974–8980.

[2] B. Kim, G. Gwak, S. Hong, Review on methodology for determining forward osmosis (FO) membrane characteristics: water permeability (A), solute permeability (B), and structural parameter (S), Desalination 422 (2017) 5–16.

[3] Y.C. Tzahi, E.C. Amy, E. Menachem, Forward osmosis: principles, applications, and recent developments, J. Membr. Sci. 281 (2006) 70–87.

[4] (a) Z. Wang, R. Sahadevan, C.N. Yeh, T.J. Menkhaus, J. Huang, H. Fong, Hot-pressed polymer nanofiber supported graphene membrane for high-performance nanofiltration, Nanotechnology 28 (2017) 31LT02;
(b) R.R. Nair, H.A. Wu, P.N. Jayaram, I.V. Grigorieva, A.K. Geim, Unimpeded permeation of water through helium-leak–tight graphene-based membranes, Science 335 (2012) 442–444.

[5] M.J. Park, S. Phuntsho, T. Heb, G.M. Nisola, L.D. Tijing, X. Lib, G. Chen, W. Chung, H.K. Shon, Graphene oxide incorporated polysulfone substrate for the fabrication of flat-sheet thin-film composite forward osmosis membranes, J. Membr. Sci. 493 (2015) 496–507.

[6] X. An, H. Ma, B. Liu, J. Wang, Graphene oxide reinforced polylactic acid/polyurethane antibacterial composites, J. Nanomater. 2013 (2013) 373414.

[7] K.Y. Wang, T.-S. Chung, G. Amy, Developing thin-film-composite forward osmosis membranes on the PES/SPSf substrate through interfacial polymerization, AICHE J. 58 (2012) 770–781.

[8] M. Hu, B. Mi, Layer-by-Layer Assembly of Graphene Oxide Membranes via Electrostatic Interaction, J. Membr. Sci. 469 (2014) 80–87.

[9] H.Q. Liang, W.S. Hung, H.H. Yu, C.C. Hu, K.R. Lee, J.Y. Lai, Z.K. Xu, Forward osmosis membranes with unprecedented water flux, J. Membr. Sci. 529 (2017) 47–54.

[10] A. Soroush, W. Ma, Y. Silvino, M.S. Rahaman, Surface modification of thin film composite forward osmosis membrane by silver-decorated graphene-oxide nanosheets, Environ. Sci. Nano 2 (2015) 395–405.

[11] H. Liu, H. Wang, X. Zhang, Facile Fabrication of freestanding ultrathin reduced graphene oxide membranes for water purification, Adv. Mater. 27 (2015) 249–254.

[12] J. Abraham, K.S. Vasu, C.D. Williams, K. Gopinadhan, Y. Su, C.T. Cherian, D. James, P. Eric, H. Sarah, V.G. Irina, C. Paola, A.K. Geim, R.R. Nair, Tunable sieving of ions using graphene oxide membranes, Nat. Nanotechnol. 12 (2017) 546–550.

[13] W. Zonghua, Y. Hairong, X. Jianfei, Z. Feifei, L. Feng, X. Yanzhi, L. Yanhui, Novel GO-blended PVDF ultrafiltration membranes, Desalination 299 (2012) 50–54.

[14] M.G. Aaron, C.S. Rodolfo, M. Hiroyuki, O.M. Josue, A. Takumi, F. Tomoyuki, T. Syogo, T. Kenji, H. Takuya, T. Mauricio, E. Morinobu, Effective NaCl and Dye rejection of hybrid graphene oxide/graphene layered membranes, Nat. Nanotechnol. 12 (2017) 1083–1088.

[15] Q. Detao, L. Zhaoyang, D.S. Darren, S. Xiaoxiao, B.A. Hongwei, New nanocomposite forward osmosis membrane custom-designed for treating shale gas wastewater, Sci. Rep. 5 (2015) 14530.

[16] D. Junjiao, Y. Yi, B. Heriberto, S. Veena, K.J. Rakesh, Mechanism of water transport in graphene oxide laminates, Chem. Sci. 8 (2017) 1701–1704.

[17] B. Radha, A. Esfandiar, F.C. Wang, A.P. Rooney, K. Gopinadhan, A. Keerthi, A. Mishchenko, A. Janardanan, P. Blake, L. Fumagalli, M. Lozada-Hidalgo, S. Garaj, S.J. Haigh, I.V. Grigorieva, H.A. Wu, A.K. Geim, Molecular transport through capillaries made with atomic-scale precision, Nature 538 (2016) 222–225.

[18] V.T. Alexandr, H. Tomas, Y. Shujie, S. Tamás, The structure of graphene oxide membranes in liquid water, ethanol and water–ethanol mixtures, Nanoscale 6 (2014) 272–281.

[19] J. Wang, K.K. Manga, Q. Bao, K.P. Loh, High-yield synthesis of few-layer graphene flakes through electrochemical expansion of graphite in propylene carbonate electrolyte, J. Am. Chem. Soc. 133 (2011) 8888–8891.

[20] (a) S.B. Jagtap, D. Ratna, Preparation and characterization of rubbery epoxy/multiwall carbon nanotubes composites using amino acid salt assisted dispersion technique, Express Polym Lett 7 (2013) 329–339;
(b) G. Mark, H. Jim, G. Ben, Just Paint, vol. 3, Golden Artist Colors Inc, New Berlin, NY, 1996, pp. 1–6 http://www.justpaint.org/wp-content/uploads/2015/11/jp03.pdf.

[21] L. Dong, J. Yang, M. Chhowalla, K.P. Loh, Synthesis and reduction of large sized graphene oxide sheets, Chem. Soc. Rev. 46 (2017) 7306–7316.

[22] A.M. Ryan, M. William, N. Derek, R.A. Thomas, J. Junghoon, P. Sung, Photoinduced force microscopy: a technique for hyperspectral nanochemical mapping, Jpn. J. Appl. Phys. 56 (2017) 08LA04.

[23] Z. Sunxiang, T. Qingsong, J.U. Jeffrey, L. Shaofan, M. Baoxia, Swelling of graphene oxide membranes in aqueous solution: characterization of interlayer spacing and insight into water transport mechanisms, ACS Nano 11 (2017) 6440–6450.

[24] J.F. Erkka, G. Lijo, E. Alexander, H. Mari, P. Jenni, L. Erkki, Measuring synthesis yield in graphene oxide synthesis by modified hummers method, Fullerenes, Nanotubes, Carbon Nanostruct. 23 (2015) 755–759.

[25] S.S. Eslah, S. Shokrollahzadeh, O.M. Jazani, A. Samimi, Forward osmosis water desalination: fabrication of graphene oxide-polyamide/polysulfone thinfilm nanocomposite membrane with high water flux and low reverse salt diffusion, Sep. Sci. Technol. 53 (2018) 573–583.

[26] X. Wu, R.W. Field, J.J. Wu, K. Zhang, Polyvinylpyrrolidone modified graphene oxide as a modifier for thin film composite forward osmosis membranes, J. Membr. Sci. 540 (2017) 251–260.

[27] Y. Wang, R. Ou, H. Wang, T. Xu, Graphene oxide modified graphitic carbon nitride as a modifier for thin film composite forward osmosis membrane, J. Membr. Sci. 475 (2015) 281–289.

[28] R. Devanathan, D. Chase-Woods, Y. Shin, D.W. Gotthold, Molecular dynamics simulations reveal that water diffusion between graphene oxide layers is slow, Sci. Rep. 6 (2016) 29484.

[29] N. Wei, X. Peng, Z. Xu, Understanding water permeation in graphene oxide membranes, ACS Appl. Mater. Interfaces 6 (2014) 5877–5883.

[30] L. Yung-Hsiang, Y. Chun-Yu, L. Sheng-Fong, L. Gong-Ru, Triturating versatile carbon materials as saturable absorptive nano powders for ultrafast pulsating of erbium-doped fiber lasers, Opt. Mater. Express 5 (2015) 236–253.